

Revisit the Oort constants measurement from *Gaia* DR2 observations and simulations

SHUFAN XIA¹

¹*Haverford College, Department of Physics and Astronomy*

1. SUMMARY

Rotation curves of disk galaxies reflect the underlying galactic mass distribution profiles. The Milky Way (WM) has a flat and slowly declining rotation curve, which indicates differential rotation - the rotation frequency varies with orbital distances. Measuring the Galactic rotation curve has remained a challenging task for astronomers. Since we are inside the MM, rotation velocities can only be derived from the relative motions of special tracers, e.g., classical Cepheid, RR Lyrae stars, and gas clouds (Levine et al. 2008, Metzger et al. 1998, Mróz et al. 2019, Wegg et al. 2019). The Oort constants measured in the solar neighborhood play an important role in bridging the local and global kinematic properties of the MM disk. While multiple measurements on Oort constants have been made, an accurate estimation requires a complete catalog of precise stellar parallax, proper motions (Kerr & Lynden-Bell 1986), and radial velocities, as well as careful considerations on the effect of different sample selections, which is still lacking. We approached this question by combing the *Gaia* DR2 data and a test particle simulation. *Gaia* DR2 catalogs parallax and proper motion measurements of over 1.6 billion stars, giving us the most comprehensive sample to calculate the Oort constants (Gaia Collaboration et al. 2016, Gaia Collaboration et al. 2018).

Assuming a thin MW disk under the cold limit and axisymmetric potential, after correcting the non-circular solar velocities about the Local Standard of Rest (LSR), (u_0, v_0, w_0) , the stellar line of sight velocity v_{los} , proper motions in the longitude and latitude directions, μ_l and μ_b , in the solar nearby region can be expressed by the Oort constants in a set of equations. The Oort constants are usually noted by A , B , C , and K , representing transverse shearing, vorticity, radial shearing, and gradient in the local velocity field. v_{los} , μ_l and μ_b all oscillate with a period of 180° as a function of Galactic longitude. Furthermore, $-(A + B)$ gives the slope of rotation curve at solar orbit, $A - B$ the local rotation frequency and $K + C$ the local gradient of radial velocity (Ogrodnikoff 1932, Binney & Merrifield 1998, Olling & Dehnen 2003).

Under the idealized circular orbits assumption, the longitudinal dependencies of μ_l , v_{los} , and μ_b are due to rotational frequency varying at the different orbital radii. In reality, potential perturbation and non-axisymmetric Galactic potential contribute to stellar non-circular velocity components, resulting in deviations from the behaviors constrained by the Oort constants. Thus, to measure the Oort constants from an extensive observational database, a critical question is how to select the best subsets of stars to derive the Oort constants - to find the proper cut-off ranges on the Galactic distance and latitude.

To answer this question, in my thesis, we first simulated a cold and thin disk and treated stars as test particles to investigate the effects of different Galactic distances and latitude ranges. Stars were sampled from the Quasi Isothermal distribution function with a vertical disk scale of 0.4 kpcs and velocity dispersion of 10 km/s to mimic a dynamically cold disk (Bovy 2015, Vasiliev 2019). We found the proper motion in the longitude direction for stars within 1 kpc from the Sun and less than 20° in their latitude is well described by the Oort constants with small deviations. If the distance or the latitude cut-off range is larger, the residuals between values derived from the Oort Constants and the actual simulated values increase with systematic deviation dependent on longitude. Similarly, a smaller range of parallax distance and latitude yields the best subset to derive the Oort constants, A , C and K from v_{los} . While μ_l and v_{los} are well described by the Oort constants when close to the MW's midplane, the latitudinal proper motion, μ_b , is expected to be significant at higher latitudes. However, in a high-latitude region, the stellar orbits are rather non-circular due to larger potential disturbance in the vertical direction. For these stars, larger vertical velocities give a more dominant contribution to μ_b than the effect from differential rotation parallel to the disk. μ_b of stars with $30^\circ \leq |b| < 50^\circ$ yield the clearest longitudinal dependency, but the dispersion and deviations are much more significant than those in μ_l and v_{los} . Thus, we concluded that it is optimal to use the μ_l and v_{los} values for stars within 1kpc and $|b| < 20^\circ$ to find the Oort constants and estimated the following values for the Oort constants: $A = 15.62 \pm 0.34$,

$B = -12.78 \pm 0.31$, $C = 1.31 \pm 0.40$, $K = 0.24 \pm 1.09$, all in the unit of km/s/kpc. These values give a rotational velocity of 238 km/s at the solar radius. We also discovered that the deviations in μ_l are due to non-zero radial velocity. In contrast, for both v_{los} and μ_b , their scattering and deviations from the Oort constants model are results of non-zero vertical velocities. The results of our test particle simulation can be seen in Fig. 1.

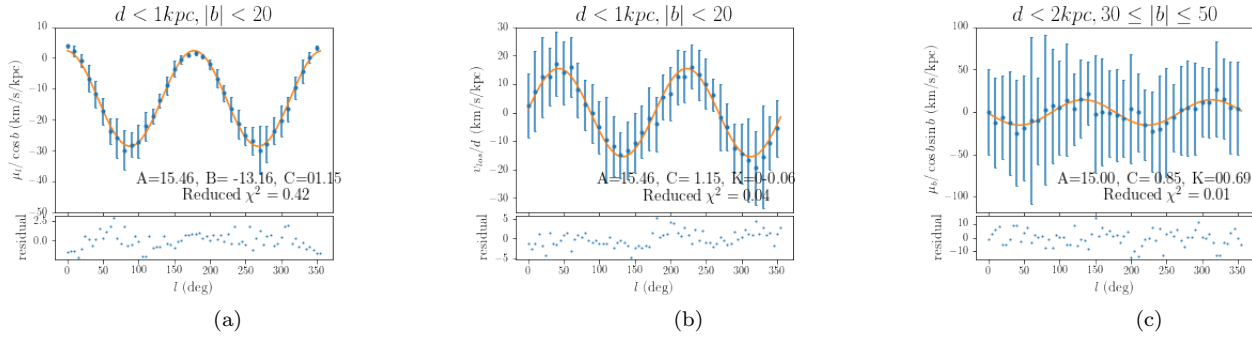


Figure 1: Test particle simulation results. The subsets that yield the best results to estimate the Oort constants from μ_l , v_{los} , and μ_b are shown. For both μ_l and v_{los} in 1a and 1b, we used stars with $d < 1\text{kpc}$ and $|b| < 20^\circ$. And for μ_b , we used stars with $d < 2\text{kpc}$ and $30^\circ < |b| < 50^\circ$. The parallax distance range for μ_b is larger because there are not enough stars within 1kpc in the above latitude range from our 500,000 test particles. In 1a), $\mu_l / \cos b = A \cos 2l + B \sin 2l + C$; 1b) $v_{los}/d = A \sin 2l + C \cos 2l + K$; 1c) $\mu_b / \sin b \cos b = A \sin 2l + C \cos 2l + K$.

For *Gaia* DR2 data, we followed the procedure laid out in the work of Bovy (2017) and Li et al. (2019). The main sequence stars are first grouped into six color groups after correcting color excess, and the Oort constants are then derived from the longitudinal profiles of μ_l , v_{los} and μ_b . We discovered that it is necessary to constraint the stars within 500 pc, a smaller range than that in the simulation, because the non-circular deviations are more significant in the real MW disk. We also found the group with the bluest stars has the slightest deviations from the models parameterized by Oort constants, while the redder color groups have more dispersion in their μ_l and μ_b , as well as larger deviations. This observation is expected because redder stars are older and have been influenced by non-circular potential perturbation for a longer time. Thus, their motions deviate more from the circular and horizontal motions constrained in the Oort constant model. Even though past works on using *Gaia* data to measure the Oort constants disregard radial velocity, we found the available radial velocities for the blue stars are abundant enough to estimate the Oort constants to a higher precision than using μ_b . The Oort constants derived from μ_l and v_{los} of these stars within 500 kpc are $A = 15.52 \pm 0.22$, $B = -13.33 \pm 0.17$, $C = -1.88 \pm 0.08$, and $K = -1.86 \pm 0.19$ in the unit of km/s/kpc, consistent with the results in Li et al. (2019) within margin of errors. The estimated slope of circular velocity at solar orbit is -18.26 ± 0.28 km/s/kpc. Fig. 2 shows the results of analyzing *Gaia* DR2.

Considering the results from our simulation and *Gaia* DR2 data, we concluded that stellar age, galactic distance, and latitude are all critical factors when sampling stars to derive the Oort constants. In addition, μ_l and v_{los} are more reliable tracers than μ_b . The conclusion from this work helps us understand the effect of sample selection on the Oort constants measurement. It can also provide some guidance on calculating the Oort constants from a larger database (*Gaia* DR3) in the near future (at the time this summary was written).

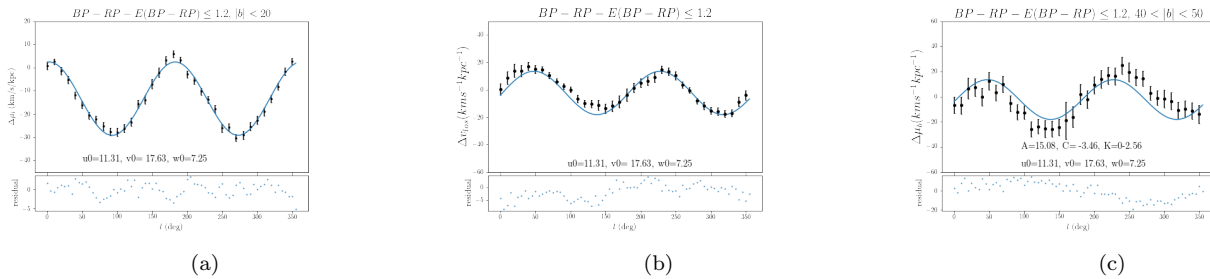


Figure 2: *Gaia* DR2 result for the blue main sequence stars within 500 pc from the Sun. 2a) $\Delta\mu_l = \frac{1}{\cos b}(\mu_l - \varpi(u_0 \sin l - v_0 \cos l) = A \cos 2l + B \sin 2l + C$; 2b) $\Delta v_{los} = \varpi(v_{los} + u_0 \cos l + v_0 \sin l) = A \sin 2l + C \cos 2l + K$; 2c) $\Delta\mu_b = -\frac{1}{\sin b \cos b}(\mu_b - \varpi[(u_0 \sin l + v_0 \cos l) \sin b - w_0 \cos b]) = A \sin 2l + C \cos 2l + K$, where (u_0, v_0, w_0) is the solar peculiar motion.

REFERENCES

- Binney, J., & Merrifield, M. 1998, *Galactic Astronomy*
- Bovy, J. 2015, *ApJS*, 216, 29,
doi: [10.1088/0067-0049/216/2/29](https://doi.org/10.1088/0067-0049/216/2/29)
- . 2017, *MNRAS*, 468, L63, doi: [10.1093/mnrasl/slx027](https://doi.org/10.1093/mnrasl/slx027)
- Gaia Collaboration, Prusti, T., de Bruijne, J. H. J., et al. 2016, *A&A*, 595, A1, doi: [10.1051/0004-6361/201629272](https://doi.org/10.1051/0004-6361/201629272)
- Gaia Collaboration, Brown, A. G. A., Vallenari, A., et al. 2018, *A&A*, 616, A1, doi: [10.1051/0004-6361/201833051](https://doi.org/10.1051/0004-6361/201833051)
- Kerr, F. J., & Lynden-Bell, D. 1986, *MNRAS*, 221, 1023,
doi: [10.1093/mnras/221.4.1023](https://doi.org/10.1093/mnras/221.4.1023)
- Levine, E. S., Heiles, C., & Blitz, L. 2008, *ApJ*, 679, 1288,
doi: [10.1086/587444](https://doi.org/10.1086/587444)
- Li, C., Zhao, G., & Yang, C. 2019, *ApJ*, 872, 205,
doi: [10.3847/1538-4357/ab0104](https://doi.org/10.3847/1538-4357/ab0104)
- Metzger, M. R., Caldwell, J. A. R., & Schechter, P. L. 1998, *AJ*, 115, 635, doi: [10.1086/300198](https://doi.org/10.1086/300198)
- Mróz, P., Udalski, A., Skowron, D. M., et al. 2019, *ApJL*, 870, L10, doi: [10.3847/2041-8213/aaf73f](https://doi.org/10.3847/2041-8213/aaf73f)
- Ogrodnikoff, K. 1932, *ZA*, 4, 190
- Olling, R. P., & Dehnen, W. 2003, *ApJ*, 599, 275,
doi: [10.1086/379278](https://doi.org/10.1086/379278)
- Vasiliev, E. 2019, *MNRAS*, 482, 1525,
doi: [10.1093/mnras/sty2672](https://doi.org/10.1093/mnras/sty2672)
- Wegg, C., Gerhard, O., & Bieth, M. 2019, *MNRAS*, 485, 3296, doi: [10.1093/mnras/stz572](https://doi.org/10.1093/mnras/stz572)